



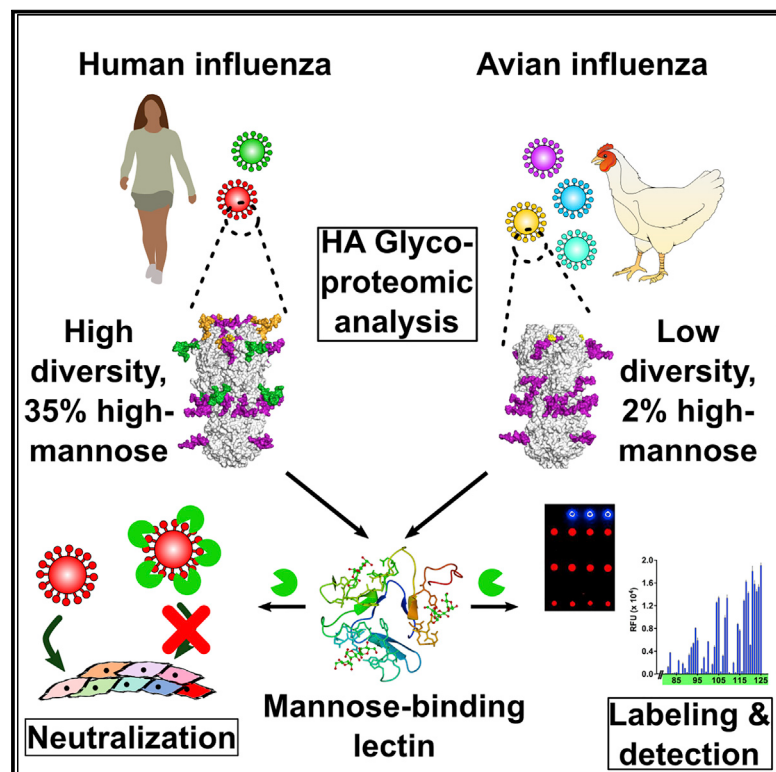
Since January 2020 Elsevier has created a COVID-19 resource centre with free information in English and Mandarin on the novel coronavirus COVID-19. The COVID-19 resource centre is hosted on Elsevier Connect, the company's public news and information website.

Elsevier hereby grants permission to make all its COVID-19-related research that is available on the COVID-19 resource centre - including this research content - immediately available in PubMed Central and other publicly funded repositories, such as the WHO COVID database with rights for unrestricted research re-use and analyses in any form or by any means with acknowledgement of the original source. These permissions are granted for free by Elsevier for as long as the COVID-19 resource centre remains active.

# Cell Host & Microbe

## Human Influenza Virus Hemagglutinins Contain Conserved Oligomannose N-Linked Glycans Allowing Potent Neutralization by Lectins

### Graphical Abstract



### Authors

Andrew J. Thompson, Liwei Cao, Yuanhui Ma, ..., Ryan McBride, John R. Yates III, James C. Paulson

### Correspondence

j.paulson@scripps.edu

### In Brief

Using site-specific glycoproteomic analysis, Thompson et al. characterize the diversity of N-glycosylation across human and avian hemagglutinin subtypes. This study reveals that hemagglutinins from human influenza viruses contain conserved glycosites with high-mannose glycosylation and demonstrates that mannose-binding lectins are useful tools for virus labeling and neutralization of H3N2 strains.

### Highlights

- Human and avian influenza hemagglutinins (HAs) have diverse glycosylation patterns
- HAs from human influenza contain conserved high-mannose type glycans
- A high-mannose-binding lectin, GNL, detects influenza HAs on glycan arrays
- GNL broadly neutralizes highly glycosylated human H3N2 strains



## Article

# Human Influenza Virus Hemagglutinins Contain Conserved Oligomannose N-Linked Glycans Allowing Potent Neutralization by Lectins

Andrew J. Thompson,<sup>1</sup> Liwei Cao,<sup>1</sup> Yuanhui Ma,<sup>1</sup> Xiaoning Wang,<sup>1</sup> Jolene K. Diedrich,<sup>1</sup> Chika Kikuchi,<sup>1</sup> Shelby Willis,<sup>1</sup> Charli Worth,<sup>1</sup> Ryan McBride,<sup>1</sup> John R. Yates III,<sup>1</sup> and James C. Paulson<sup>1,2,3,\*</sup>

<sup>1</sup>Department of Molecular Medicine, Scripps Research, La Jolla, CA 92037, USA

<sup>2</sup>Department of Immunology & Microbiology, Scripps Research, La Jolla, CA 92037, USA

<sup>3</sup>Lead Contact

\*Correspondence: [jpaulson@scripps.edu](mailto:jpaulson@scripps.edu)

<https://doi.org/10.1016/j.chom.2020.03.009>

## SUMMARY

Hemagglutinins (HAs) from human influenza viruses adapt to bind  $\alpha$ 2-6-linked sialosides, overcoming a receptor-defined species barrier distinct from the  $\alpha$ 2-3 specificity of avian virus progenitors. Additionally, human-adapted HAs gain glycosylation sites over time, although their biological function is poorly defined. Using quantitative glycomic analysis, we show that HAs from human pandemic viruses exhibit significant proportions of high-mannose type N-linked glycans throughout the head domain. By contrast, poorly adapted avian-origin HAs contain predominately complex-type glycans, which have greater structural diversity. Although oligomannose levels vary, they are present in all tested recombinant HAs and whole viruses and can be specifically targeted for universal detection. The positions of high-mannose glycosites on the HA of human H1N1 and H3N2 strains are conserved. Additionally, high-mannose-binding lectins possess a broad capacity to neutralize and prevent infection with contemporary H3N2 strains. These findings reveal the biological significance of HA glycosylation and therapeutic potential of targeting these structures.

## INTRODUCTION

Influenza A viruses (IAVs) are a leading cause of severe respiratory disease and death. IAVs pose a threat, particularly to human health, through the continual emergence of seasonal epidemics and occasional global pandemics (Krammer et al., 2018; Paules and Subbarao, 2017). The epidemiological “success” of IAVs depends on their ability to efficiently infect and subsequently transmit among host individuals, typically via airborne respiratory droplets (Killingley and Nguyen-Van-Tam, 2013; Neumann and Kawaoka, 2015). To combat this danger, significant resources have been deployed to establish global networks for detecting, sequencing, and surveilling potentially hazardous IAV strains, both within humans and other species (Ziegler et al., 2018).

Human IAVs comprise three strains: H1N1, H2N2, and H3N2, which were introduced into the population from avian and swine species during pandemic outbreaks over the last century (Garten et al., 2009; Smith et al., 2009; Webster et al., 1992). While hemagglutinins (HAs), from human IAVs bind specifically to N-acetyl-neurameric acid (sialic acid) linked  $\alpha$ 2-6 to galactose (Neu5Ac $\alpha$ 2-6Gal) present on human upper airway cells, HAs from avian IAV strains preferentially recognize  $\alpha$ 2-3-linked sialosides (Neu5Ac $\alpha$ 2-3Gal) (Connor et al., 1994; Rogers and Paulson, 1983). This divergence of receptor structures and/or chemistries forms a protective “species barrier,” preventing transmission and circulation of avian IAV subtypes within humans without adapting to human-type receptors (de Graaf and Fouchier,

2014; Imai and Kawaoka, 2012). The H1, H2, and H3 HAs of avian virus progenitors responsible for these pandemics required only one- or two-amino acid mutations in the receptor-binding site (RBS) to achieve a switch from avian to human-type receptor specificity (Connor et al., 1994; Rogers et al., 1983; Tumpey et al., 2007). In addition to well-studied specificity changes, “humanized” HAs have been shown to acquire other adaptations including increased thermal stability, decreased fusion-pH, and increased N-linked glycosylation (Linster et al., 2014; Zhang et al., 2004). While many of these changes reflect escape from immune responses or represent adaptative alterations to improve binding, infection, and replication in human cells, the role of additional glycans, and particularly details of their composition and structure, remain comparatively under-investigated. Indeed, only two recent literature examples report site-specific and quantitative analysis of N-linked glycans from representative influenza HAs providing limited information with regard to the impact of species of origin and evolution during passage in humans (Khatri et al., 2016; Parsons et al., 2017).

Here, we report a more comprehensive site-specific analysis of N-linked glycans from contemporary IAVs comprising six evolutionarily distinct hemagglutinin subtypes: H1, H3, H5, H6, H7, and H10 from human and avian influenza viruses. We find that HA stem-domain glycosites conserved across all subtypes exhibit extensive processing of glycans from a high-mannose to complex-type, while glycosites within the head domain of human HAs, including those added incrementally over time,



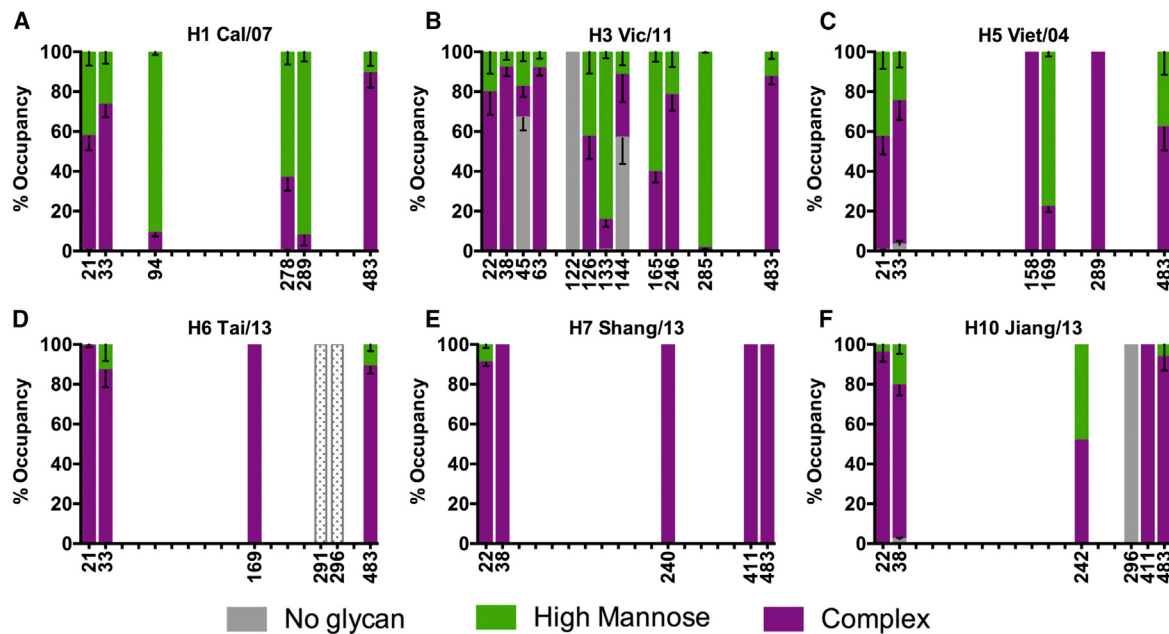


**Figure 1. Glycoproteomic Analysis of Diverse Influenza Virus HAs**

Shown is the glycosylation status of each HA N-linked glycosite (Asn-X-Thr/Ser) with either complex type (purple), high-mannose or hybrid type (green), or no glycan (gray), at individual positions within Cal/07 H1 (A), Vic/11 H3 (B), Viet/04 H5 (C), Tai/13 H6 (D), Shang/13 H7 (E), and Jiang/13 H10 (F). Bars are distributed along the x axis according to relative position in the primary sequence, with specific glycosites depicted by numbering of the glycosylated asparagine (N). Two glycosites in H6 for which corresponding glycopeptides could not be detected in the MS analysis are shown as open gray bars. A glycosite at position N8 in Vic/11 H3 has been excluded due to protein stability, all H3 constructs include only the folded ectodomain (residues 11–521). Histograms depict average occupancy with error bars showing standard error.

exhibit significant oligomannose-type glycans with minimal processing. Consistent with the presence of conserved oligomannose glycans on influenza HAs, we show that, even when present at low frequencies, a high-mannose-specific lectin from *Galanthus nivalis* (GNL; snowdrop lectin) (Kaku and Goldstein, 1989) can be used for universal labeling and detection of whole IAVs and recombinant HAs on sialoside microarrays, without the requirement for specific antiviral reagents, such as monoclonal antibodies or antisera. Moreover, GNL was also able to inhibit receptor binding and broadly neutralize recent human H3N2 viruses with either comparable or superior potency to a panel of antiviral antibodies. Energy-minimized modeling of glycosylated crystal structures for all six representative HAs reveals conservation of both the positions and types of glycans at individual glycosylation sites, particularly within the group 1 and 2 HA phylogenetic classes (Air, 1981; Nobusawa et al., 1991). Comparison of the glycosylated HAs suggests overall location on HA, together with local structural features surrounding the glycosites to be the major determinants of oligomannose glycoforms, rather than dense packing of multiple sites, as observed in other viruses, such as the human immunodeficiency virus (HIV) (Cao et al., 2017, 2018). Structural mapping of high-mannose glycans in the HA of human H3N2 viruses reveals the presence of a small high-mannose patch, in close proximity to the RBS at the top of H3, accounting for the effectiveness of GNL neutralization. Insights into immune recognition of glycosylated HAs, vaccine production and development, and universal virus detection via surface glycans are discussed in light of these findings.

## RESULTS

### Influenza HAs from Diverse Subtypes Exhibit Substantial Differences in N-Linked Glycan Processing

To investigate differences in IAV glycosylation, we performed global site-specific analysis of glycan occupancy and degree of processing from high-mannose to complex-type glycans for all potential N-linked glycosylation sites present on six representative HA ectodomains from both human and avian IAVs, including: A/California/07/2009 (pH1N1, human 2009 pandemic; Cal/07), A/Victoria/361/2011 (H3N2, human seasonal; Vic/11), A/Viet Nam/1203/2004 (H5N1, avian origin; Viet/04), A/Taiwan/2/2013 (H6N1, avian origin; Tai/13), A/Shanghai/2/2013 (H7N9, avian origin; Shang/13), and A/Jiangxi Donghu/346/2013 (H10N8, avian origin; Jiang/13). These strains were selected to include HAs from two contemporary human IAV strains (H1N1 and H3N2) and four avian IAVs, which together comprise the two major HA phylogenetic subgroups, group 1 (H1, H5, and H6) and group 2 (H3, H7, and H10). This proteomics-based method for site-specific analysis of N-linked glycan processing uses endoglycosidases to introduce mass signatures that contain either no glycan, minimally processed high-mannose or hybrid-type, or more extensively processed complex-type N-glycans. This allows a semi-quantitative assessment of the proportion of each glycoform present at each glycosite (Cao et al., 2017, 2018).

The results reveal differences in glycosylation between individual HAs, and particularly between human and avian IAVs (Figure 1). Both of the human HAs, Cal/07 (H1) and

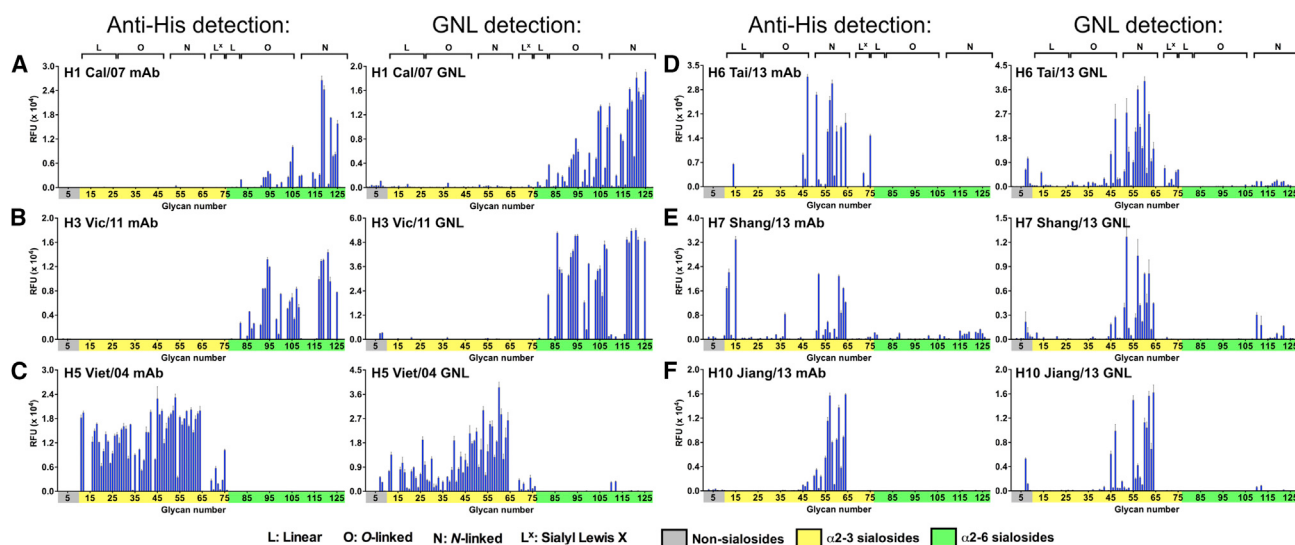


**Figure 2. Comparison of GNL versus Anti-His Staining of Recombinant HAs on the Glycan Array**

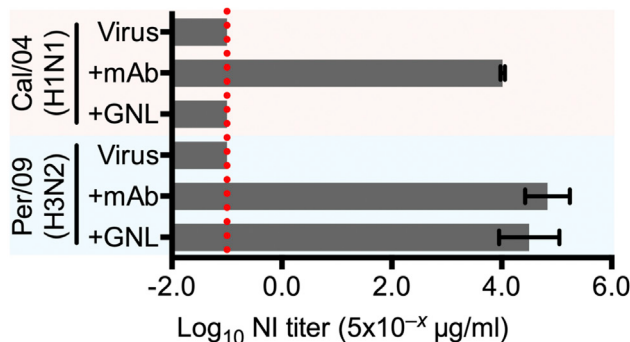
(A–F) Direct staining of high-mannose glycan on recombinant HA trimers with GNL (right panels) gives strongly comparable data to traditional anti-His staining (left panels) for all HAs: Cal/07 H1 (A), Vic/11 H3 (B), Viet/04 H5 (C), Tai/13 H6 (D), Shang/13 H7 (E), and Jiang/13 H10 (F). Particularly relevant for universal virus receptor specificity analysis, GNL robustly detects HAs of human and avian IAVs, even those with low content of high-mannose glycans. Bars depict mean intensity minus mean background of the four median out of six total replicate observations with error bars showing standard error.

Vic/11 (H3) (Figures 1A and 1B), exhibit a large proportion of high-mannose type glycans, particularly at glycosites on the HA head domain, which also contains the RBS. Conversely, the majority of glycosites present on avian-derived HAs are uniformly more processed to complex-type glycans (Figures 1C–1F). Interestingly, although contemporary human H3 HAs are regarded as “highly glycosylated” (Vic/11 has 13 potential glycosites), we observed that one position (N122) is entirely unoccupied, and a further two sites (N45 and N144) are occupied by a glycan less than 50%, suggesting that H3 HAs on average have a more modest 11–12 fully occupied glycosites, in line with recent proposals of a HA glycan saturation limit (Altman et al., 2019). Several poorly occupied glycosites in Vic/11 H3 and a single unoccupied site at N296 (H3 numbering, used here and throughout) in Jiang/13 H10 fall in close proximity to other glycosites in the primary amino acid sequence (Figures 1B and 1F). Similarly, the adjacent glycosites at positions at N278 and N289 in Cal/07 H1, N126 and N133 in Vic/11 H3, and N158 and N169 in Viet/04 H5 appear to result in minimal processing, with at least one glycosite of each pair observed as oligomannose-type (Figures 1A–1C). Notably, however, glycan crowding is not the only reason for under-processing of glycans since isolated glycosites at N94 in Cal/07, N165 and N285 in Vic/11, and N242 in Jiang/13 display significant proportions of high-mannose glycans (Figures 1A, 1B, and 1F), suggesting that the architecture of the folded HA structure may also influence the extent of glycan processing. All six HAs have a conserved glycosite at N483 that is predominantly complex type (Figure 1), while group 1 HAs (H1, H5, and H6) contain a pair of predominantly complex glycans at N21 and N33, and group 2 HAs (H3, H7, and H10) feature a directly comparable pair of glycosites at positions N22 and N38, also found to be mostly complex type (Figures 1A–1F).

### High-Mannose-Specific GNL Lectin Enables Robust Labeling of Influenza HA

Although the analyzed HAs contained variable amounts of high-mannose type glycans, all included at least low levels of oligomannose, raising the possibility that they could be specifically labeled by a mannose-selective lectin, and subsequently used for detection. GNL is a commercially available, non-Ca<sup>2+</sup>-dependent lectin with specificity for  $\alpha$ 1-3-linked mannoside sugars found in high-mannose type N-glycans, making it a candidate to detect HAs and IAVs in glycan array experiments. While our glycan arrays contain N-linked glycans with a Man<sub>3</sub>GlcNAc<sub>2</sub> core, GNL does not appear to be able to bind complex-type glycans with terminal sialic acids and gave minimal background reactivity with sialylated N-linked glycans on the array (Figure S1A; for a list of array glycans see Data S1). To assess detection of purified IAV HAs, the same panel of six human and avian HAs used for MS analysis were applied to microarrays, either as a pre-incubated complex with anti-His and AF488-labeled secondary antibodies (standard protocol, see STAR Methods) or by direct incubation of pure HA trimers on the microarray surface, followed by washing and incubation with a pre-formed complex of biotinylated GNL and AF488-labeled streptavidin. Detection of bound samples via GNL staining of high-mannose glycans was comparable to that achieved with antibodies in all cases, with specificity patterns and binding fingerprints appearing qualitatively matched (Figure 2). Furthermore, GNL detection was also able to enhance signals of weaker-binding glycans, presumably due to more robust staining of multiple high-mannose glycosites per trimer.

To examine utility of GNL as a serology-independent reagent for labeling whole IAV samples, we analyzed a subset of four viruses: A/California/04/2009 (pH1N1; Cal/04), Vic/11, and A/Anhui/1/2013 (H7N9; Anhui/13), with close similarity to recombinant

**A****B**

mAb Clone:	Bris/07	Per/09	Vic/11	Switz/13	HK/14
$\alpha$ Bris/07	6.32E-03	>20	0.063	>20	0.063
	0.063	>20	>20	>20	>20
	0.063	>20	>20	>20	2
	0.063	>20	0.063	>20	>20
$\alpha$ Per/09	>20	6.32E-05	6.32E-04	0.063	>20
	>20	4.69E-03	6.32	>20	>20
$\alpha$ Vic/11	>20	>20	>20	>20	>20
	>20	6.32E-04	0.063	>20	>20
	0.047	0.063	0.063	0.063	>20
	>20	4.69E-04	6.32E-03	0.063	0.083
	>20	8.34E-04	6.32E-03	6.32E-03	>20
GNL	6.32E-05	8.34E-05	6.32E-04	0.063	0.083

HA samples investigated above, plus a pre-pandemic human seasonal strain, A/New Caledonia/20/1999 (H1N1; NC/99). Despite their distinct antigenicities, when detected with GNL, specific binding to the array was clearly observed for all virus samples (Figures S1B–S1E). Both Cal/04 and Vic/11 virus samples maintain closely matched receptor specificity to purified HA counterparts in Figures 2A and 2B. For Anhui/13 and NC/99, we also sought to compare glycan-specific labeling with serological methods for detection, including an antiviral mouse antibody (Anhui/13) and sheep-derived antisera (NC/99). Again, GNL reproduced receptor specificities identified by serological staining, with Anhui/13 showing mixed linkage preferences for both  $\alpha$ 2-3 and  $\alpha$ 2-6-linked N-glycans, and NC/99 appearing majority  $\alpha$ 2-6 specific with minor interactions with some  $\alpha$ 2-3 receptors (Figures S1D and S1E). Since labeling with GNL offers comparable data to antibody or antisera-based detection, this method may provide a simple future alternative for detection of HAs and IAVs in glycan-binding assays when specific antiviral reagents are not available.

### High-Mannose Glycans in H3N2 IAVs Are a Potential Target for Neutralization

Since both human H1N1 and H3N2 viruses feature high-mannose glycans at potentially key positions within the HA head domain, we investigated the ability of GNL to inhibit receptor binding and neutralize infection *in vitro* using cell culture microneutralization (MN) and hemagglutination inhibition (HAI)

**Figure 3. GNL Binding to High-Mannose Glycans Broadly Neutralizes Recent H3N2 Viruses**

(A) Virus microneutralization of assays of whole Cal/04 (H1N1) and Per/09 (H3N2) viruses pre-treated with either PBS, anti-Cal/04 mAb, anti-Per/09 mAb, or GNL. Bars depict average titers with error bars showing standard deviation.

(B) Broad virus microneutralization assays, utilizing an expanded panel of five recent H3N2 vaccine strain viruses and eleven specific antiviral mouse monoclonal antibodies raised against recombinant HA from three viruses, and GNL. Shown are respective virus neutralization titers as bars (A) or with cells colored in red according to neutralization potency (B). GNL neutralizes all H3N2 viruses tested, with comparable or superior strength to the best mAb but does not neutralize Cal/04 H1N1.

assays (Figures 3 and S2). Relative to a specific anti-H1 monoclonal antibody (mAb) with known MN function, GNL failed to protect Madin-Darby canine kidney (MDCK) cells from infection with Cal/04 (H1N1) virus, suggesting that the observed high-mannose glycans are located some distance from the RBS (Figure 3A). Conversely, however, GNL showed potent neutralization of Per/09 (A/Perth/16/2009; H3N2) compared with a control anti-H3 mAb (Figure 3B), indicating that at least one oligomannose site in the more-heavily glycosylated H3 head is likely suitably positioned for strong inhibition of receptor engagement. Comparable data were also obtained for HAI assays, where GNL showed successful inhibition of Per/09 only, while comparison of GNL with a panel of lectins with diverse glycan specificities revealed potent neutralization to be confined to high-mannose-targeted reagents only (Figure S2).

To investigate the potential for broad neutralization of H3N2 viruses, we conducted expanded MN screening against five recent human H3N2 vaccine strains and a panel of eleven mAbs raised against the HAs from three of these strains, plus GNL (Figure 3B). Selected H3N2 IAVs included: Bris/07 (A/Brisbane/10/2007), Per/09, Vic/11, Switz/13 (A/Switzerland/9715293/2013), and HK/14 (A/Hong Kong/4801/2014). As expected, various mAb clones exhibited neutralization in a mainly strain-specific manner, generally favoring the parent IAV or HA against which they were raised, with the exception of anti-Vic/11 clone FR1122, which failed to neutralize any IAV tested (Figure 3B). All four anti-Bris/07 mAbs weakly neutralized Bris/07, while two, FR509 and 512, showed similar cross-neutralization of Vic/11 (509 and 512) and HK/14 (509 only). Correspondingly, one anti-Vic/11 mAb (FR1124) showed similar neutralizing titer against Bris/07, suggesting a shared epitope shared between the two viruses. Interestingly, despite evolving between Bris/07 and Vic/11, Per/09 appears to show little cross-reactivity with anti-Bris/07 mAbs (and vice versa), despite highly potent neutralization by both anti-Per/09 and anti-Vic/11 species (Figure 3B). Vic/11 was

the most widely neutralized virus, revealing mainly weak titers against eight out of eleven mAbs tested. Interestingly, however, anti-Vic/11 mAbs appeared to give strongest MN titers against Per/09 virus, although observed titer differences of generally 1-log or less are comparatively small within the context of this assay. In terms of broad neutralization, none of the antiviral mAb samples tested were able to neutralize all five H3N2 strains. Two anti-Vic/11 clones, FR1124 and 1125, neutralized four of five viruses with generally weak potency. Unsurprisingly, given their later appearance in evolution and likely advanced antigenic drift, Switz/13 and HK/14 were only relatively weakly neutralized—with Switz/13 sharing reactivity with closely related anti-Vic/11 mAbs, and HK/14 with one anti-Vic/11 and one anti-Bris/07 sample.

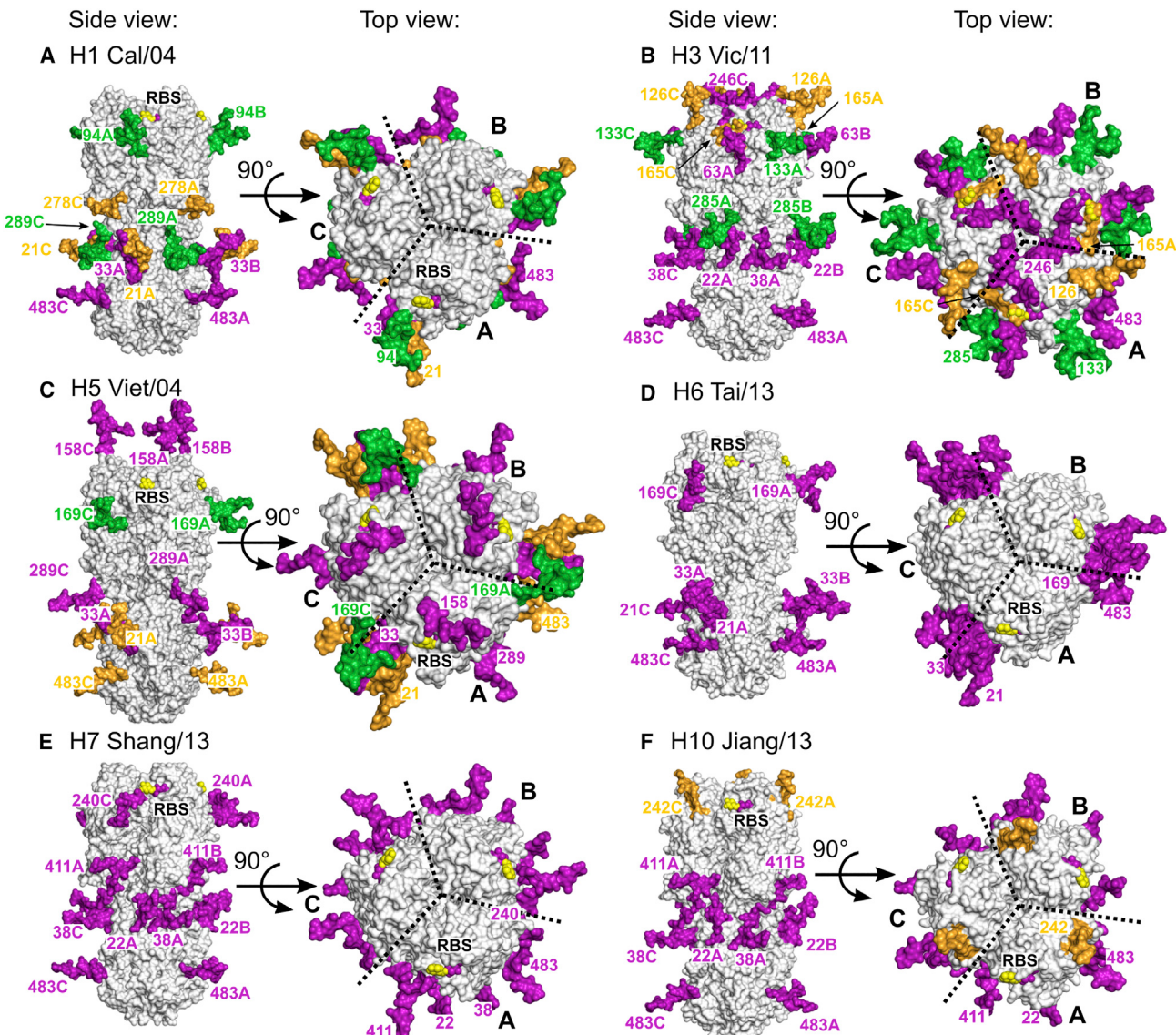
In contrast to the limited neutralization of the virus panel by mAbs, GNL targeting of high-mannose glycans gave consistently strong neutralization. Indeed, GNL showed neutralizing activity, independent of underlying sequence and antigenic drift variants, against all five virus samples examined, with MN titers comparable to the best specific mAbs for each virus (Figure 3B). Together, these data suggest that consideration of specific glycan epitopes within vaccine design (such methods are prominent within the HIV field [Andrabi et al., 2018]) could enhance both efficacy and broad protection, especially within human IAV strains where glycosites accumulate and oligo-mannose species appear conserved across the HA head domain.

### High-Mannose Glycosites Map to the Antigenically Dominant HA Head Domain

Quantitative glycoproteomics data (Figure 1) reveal the presence of high-mannose type glycosites in both the H1N1 and H3N2 human IAV strains; however, GNL neutralized only H3N2 virus (Figure 3), implying differences in the localization of high-mannose glycans within the two strains. To better understand such glycosylation differences, we set out to look at the glycosylation data for the six HAs in Figure 1 in the context of their three-dimensional structures. Due to their conformational flexibility, HA glycans are not typically found in crystal or cryo-electron microscopy structures deposited in the PDB. We therefore employed a computational approach to assign energy-minimized glycan structures and conformations *de novo* at glycosites on the recombinant HAs (see STAR Methods and Figure S3A). Shown in Figure 4 are the top and side views of each of the six HA subtypes, with energy-minimized glycan structures modeled at each glycosite, and colored according to the dominant glycan type determined by MS (Figure 1). Predominantly high-mannose and complex-type glycans are shown in green and purple, respectively, while sites with at least 30% of each type are designated “mixed” and colored orange. Sites with substantial high-mannose content (green) are present only in H1, H3, and H5, and are located exclusively within the HA1 subunit, with the vast majority found adorning the antigenically dominant head domain that contains the RBS (Figures 4A–4C). While further broad similarities among the panel are mainly confined to subgroups, e.g., within human or avian origin, or phylogenetic group 1 and 2 HAs, all six HAs contain one mainly complex-type glycan at N483 that occupies a very similar conformation (Figure 4).

Covering the interface between the head and stem domains in all HAs, there is a reasonably conserved “glycan ring” composed mainly of complex glycosites. These glycans include the comparable pairs of N21 and N33 (group 1 HAs), and N22 and N38 (group 2 HAs), N278 (H1), N285 (H3), N289 (H1 and H5), and N411 (H7 and H10). The glycan ring appears to form a relatively closed shield, obstructing access to the top of the stem domain that forms the core of the HA membrane-fusion machinery. Within Cal/04 H1 (Figure 4A), the ring harbors two predominantly high-mannose glycosites, N278 and N289, located immediately at the head-stem interface. A similarly located glycosite in Vic/11 H3, N285, is also predominantly high-mannose (Figures 1B and 4B), while N289 in avian Viet/04 H5 is 100% complex type (Figures 1C and 4C). Although Cal/04 N289 is somewhat close to N278 in the primary sequence, suggestive of hindrance to processing by  $\alpha$ -mannosidases, structural analysis suggests this region to be uncrowded in both H1 and H5 (Figures 4A and 4C). Sequence and structural alignments reveal subtle differences around the Cal/04 and Viet/04 N289 positions that may account for the strong divergence in attached glycoforms (Figure 5). Within Cal/04 H1, the N289 glycosite comprises an “NTS” glycosylation sequon, compared with “NSS” in Viet/04 (Figure 5A). In the Cal/04 structure, the hydrophobic methyl group on T290 appears rotated into a small hydrophobic pocket created by the side chains of T280 and P306, leading to a rearrangement of the amino acid backbone relative to Viet/04 and an approximate 45-degree rotation of the N289 side chain in toward the protein surface (Figures 5B and 5C). Final energy-minimized models of the glycosylated form of Cal/04 N289 reveal that the attached glycan lies closely packed against the HA surface, rather than in an extended solvent-accessible form as for Viet/04 (Figure 5D), likely contributing to reduced access for processing and the consistent observation of a high-mannose species at this position. Similar structural variances are also evident for Cal/04 N94, whose location within a shallow pocket beneath the major part of the head domain and proximal to the trimer interface, appears to result in a similar high-mannose glycoform closely contacting the HA surface (Figure S3B).

Above the glycan ring most HAs are quite undecorated, particularly those of avian origin (Figures 4D–4F). Tai/13 H6 and Shang/13 H7 present with the simplest and most homogeneous glycosylation, maintaining both minimally decorated head domains and mainly complex glycans at every observed glycosite (Figures 4D and 4E). Interestingly, while the glycosylation profile (see Figure 1) of Tai/13 is most closely matched to Shang/13, the location of all four observed glycosites is most closely conserved in Viet/04 H5 (Figures 4C and 4D), however, the attached species vary strongly. Interestingly, structural or positional variances that might impair mannosidase processing in Viet/04, relative to Tai/13, are less readily observed than in H1 and H5, with glycan conformations in respective glycosylated structures appearing highly similar (Figure S3C). Within group 2 HAs, Shang/13 H7 and Jiang/13 H10 feature several matched or comparable glycosites, including predominantly complex-type glycans at N22, N38, N411, and N483 (Figures 4E and 4F). Shang/13 and Jiang/13 also contain one comparably positioned glycan with heterogeneous occupancy at N240 and N242, respectively (N240 is 100% complex in H7, while N242

**Figure 4. Energy-Minimized Glycosylated HA Structures from MD Simulations**

(A–F) Glycomics data determined in Figure 1 were used to inform modeling of likely glycan structures at each individual glycosite across all six HA candidates: Cal/04 H1 (A), Vic/11 H3 (B), Viet/04 H5 (C), Tai/13 H6 (D), Shang/13 H7 (E), and Jiang/13 H10 (F) using GLYCAM. Figures depict complete HA trimeric ectodomains (shown as gray surface models) in side view (left) and top view (right). The structure and position of individual N-glycans are shown as color-coded surfaces: >70% complex (purple), >70% high-mannose/hybridG (green), and mixed occupancy (orange) and are labeled according to the protomer they belong to (either A, B, or C; see top view). The trimer interface in each HA is defined by broken lines in top view. Unoccupied (no glycan) or unobserved (glycopeptides that could not be detected) glycan positions are not modeled. The location of the RBS is labeled for each HA and a bound Neu5Ac-Gal disaccharide (purple and yellow spheres) modeled within each for illustration. Complex, high-mannose, al and NeuAc species color schemes are according to the Consortium for Functional Glycomics (CFG) guides for Neu5Ac, mannose, and galactose, respectively.

is only 51% complex in H10; Figure 1). Glycosylated models of N240 and N242 reveal that the attached glycoforms possess very different conformations, with Shang/13 N240 pointing directly out from the HA surface in an open conformation, while Jiang/13 N242 projects directly up toward the top of HA, and packs closely against the protein surface, potentially reducing access for processing (Figure S3D).

The top of the HA molecule is relatively undecorated in most viral subtypes, with the exception of H5 and recent human H3 vi-

ruses (Chambers et al., 2015; Zost et al., 2017) (Figures 4B and 4C). Viet/04 possesses a complex-type glycan at N158, which projects directly out and above the molecule, and while likely an antigenic adaptation, has also been shown to be a major obstacle for  $\alpha$ 2-6 receptor binding (Herfst et al., 2012; Imai et al., 2012). The top of Vic/11 H3 is densely covered by multiple glycans and contains fully occupied glycosites at N63, N126, and N133, and partially occupied species at N45 and N144, that are not observed in other HAs (Figure 4B). Interestingly,

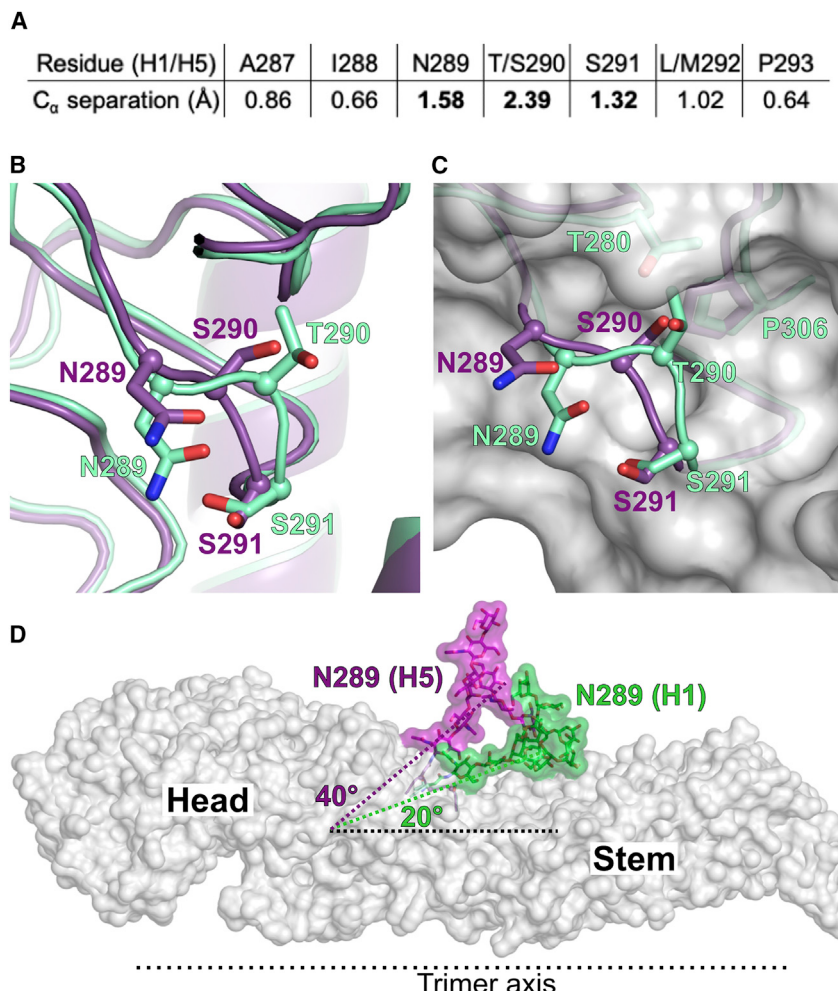


**Figure 5. Structural Comparison of a Matched High-Mannose versus Complex Glycosite in H1 and H5 HAs**

(A and B) Cal/04 H1 and Viet/04 H5 show strong structural and sequence conservation around the N289 glycosite (A, top line and B) with the exception of position 290 at the center of the N-glycosylation sequon. Substitution of S290 in H5 for T290 in H1 leads to structural deviation of the amino acid backbone (A, lower line, separation of matched C<sub>α</sub>s is maximal at position 290) as the hydrophobic side chain becomes rotated into the HA surface (B; H1 colored green, H5 in purple).

(C) shows an alternate view with HA residues around the glycosite shown as gray surface. Here, H1 T290 (green) is positioned closer to the hydrophobic rear face of T280 and the side chain of P306.

(D) To counter distortion of the backbone structure caused by T290, the side chain of N289 is rotated down and in toward HA by approximately 45 degrees, leading to a shift in conformation of the N289 glycan. MD simulations predict that the chitobiose core of the N-glycan in H1 becomes shifted approximately 20 degrees closer to the protein surface, likely creating steric hindrance to glycan processing. Glycans in (D) are shown in green surface for high-mannose in H1 and purple surface for complex type in H5.

the structure and location of two significant high-mannose glycosites in Vic/11, N165 and N285, are analogous to oligomannose sites in H1 and H5 (compare Figures 4A–4C), while a third unique site, N133, is positioned nearby, creating the appearance of a “high-mannose patch” (Figure 4B). While all three of these glycans appear close to the RBS, the modeled high-mannose glycan at N165 lies extremely nearby and appears the most likely target for neutralization by GNL. That N165 and N285 are conserved in all H3 HAs since 1968 (Figure S4) also provides a rationale for observed broad neutralization within this group. All modeled high-mannose glycans in Vic/11 H3 appear to pack closely against the surface of the HA molecule, similar to those described above. Together, these data suggest a model whereby IAVs, particularly those associated with human infection, select for increased glycosylation around the HA head domain, and that evolution of predominantly high-mannose species at particular glycosites may be controlled by structural and/or sequence features within HA itself.

## DISCUSSION

Through minor evolutionary drift of human seasonal strains and major reassortments of avian viruses, IAVs pose a significant and

complex challenge to health (Krammer et al., 2018; Paules and Subbarao, 2017). Zoonotic IAV strains adapt to transmission among human hosts initially through changes in receptor specificity, increased HA stability, replication-enhancing polymerase mutations, and, subsequently, through antigenic drift within the HA head and addition of head-domain glycans. While research

in many of these areas has matured significantly during the last decade, particularly with respect to receptor specificity switching (Chen et al., 2012; de Vries et al., 2017a, 2017b; Srinivasan et al., 2013; Tzurum et al., 2017; Yamada et al., 2006), details of IAV glycosylation and evolutionary or adaptive changes to the HA glycome remain poorly understood. This is in-part due to substantial technical challenges, meaning many studies employ non-site-specific or poorly quantitative techniques to interpret glycosylation patterns, while more advanced methods have proved labor-intensive and extremely low-throughput, revealing only limited insights. Knowledge of HA glycosylation and links to antigenicity are of increasing interest, since despite long-running immunization programs, development of effective and broadly protective IAV vaccines has remained difficult and represents a major research goal (Erbelding et al., 2018).

In this study, we demonstrated variably heterogenous glycosylation patterns within a diverse panel of HAs, ranging from minor high-mannose fractions in avian HA stem domains, to near-complete oligomannose sites within the heads of human IAV HAs. Glycoproteomics analysis and structures of glycosylated HAs highlight broad conservation as to the location of many HA glycans, while occupancy of these sites with either complex or high-mannose glycoforms appears far more diverse,

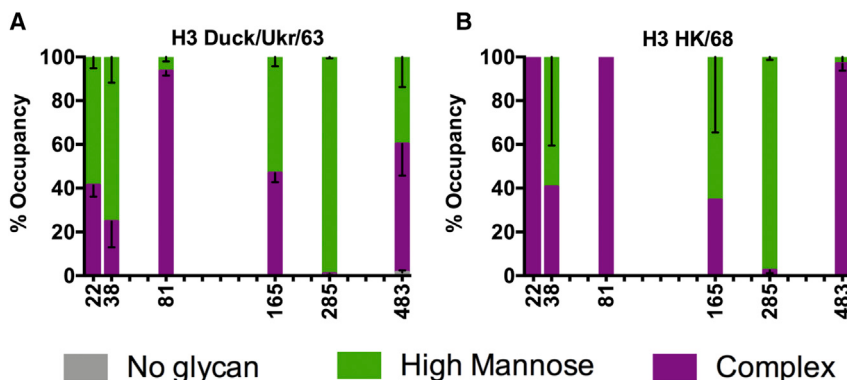


**Figure 6. Quantitative Glycomic Analysis of H3 Precursors**

All graphs show percentage occupancy of specific N-linked glycoconjugates with either complex type (purple), high-mannose or hybrid type (green), or no glycan (gray), at individual glycosites within A/Duck/Ukraine/1/1963 (A; H3 precursor to 1968), and A/Hong Kong/1/1968 (B; 1968 H3N2 pandemic strain). Bars are distributed along the x axis according to relative position in the primary sequence, with specific glycosites depicted by numbering of the glycosylated asparagine (N). Histograms depict average occupancy with error bars showing standard error.

particularly between avian and human examples. That highly occupied oligomannose sites are almost exclusively associated with human-adapted HAs, suggests the possibility that reduced glycan processing might be selected for as part of host adaptation. Notably, glycosites with significant oligomannose content such as N94 and N289 in H1, and N165 and N286 H3, are well-conserved since the respective emergences of both H1N1 and H3N2 IAVs in humans (Figure S4). Further glycoproteomic analysis of two early H3 HAs from A/Duck/Ukraine/1/1963 (DK/63; avian H3 precursor) and A/Hong Kong/1/1968 (HK/68; human pandemic H3) strongly supports this possibility, revealing that both H3 precursors also contain significant high-mannose fractions at N165 and N285 (Figure 6). Interestingly, with significant oligomannose fractions detected at all glycosites, the avian H3 pandemic precursor DK/63 appears quite distinct from contemporary avian examples profiled. Thus, appearance of high-mannose type glycans on IAV HAs may well be more complicated than simple host origin or adaptation. However, while the H5, H6, H7, and H10 HAs investigated here do reflect avian IAVs that have been able to infect humans in isolated cases, none have yet fully evolved properties to enable sustained human-to-human transmission. Comparison of glycome profiles determined here with additional examples in the literature (Khatri et al., 2016; Mir-Shekari et al., 1997; Nakamura et al., 1980; Ward and Dopheide, 1981a, 1981b; Ward et al., 1980) (see Figure S5) further supports observations that certain high-mannose glycoforms are well-conserved in fully adapted human H1 and H3 HAs, even between very early and late examples. Together these data suggest a model where IAVs carrying high-mannose glycans may be predisposed to human adaptation, or that host-adaptive pressures may instead select for strains with potential for increased high-mannose incorporation.

While an exact evolutionary driver is unclear, several potential selective advantages conferred by a shift to favor high-mannose glycosylation in human IAVs can be observed. For example, modeling analyses suggest that high-mannose type glycans mostly favor close packing against the HA surface. Glycans in such a conformation have potential as a steric shield, and are suggested here since almost all glycosites with significant oligomannose fractions map to functionally important regions of HA such as key antigenic sites, and the interface of the head and stem domains which houses the membrane-fusion machinery (Blijlevens et al., 2016) (Figure 4). Steric blocking at this interface region, which has high sequence homology across all HA sub-

types, would likely confer advantage on human seasonal IAV strains, biasing antibody responses to more exposed areas of the viral surface with greater tolerance to antigenic drift. Additionally, the altered presentation of glycoepitopes where high-mannose glycans are attached might also reduce immunogenicity by altering or inhibiting antibody recognition of the more recessed carbohydrate component. Increased high-mannose glycosylation may also provide a replicative advantage during infection, since treatment of MDCK cells with the ER  $\alpha$ -mannosidase inhibitor kifunensine has been shown to lead to enhanced growth and replication (Elbein et al., 1982; Pan et al., 1983). One recent report has suggested that this effect may center around specific induction of the ER-associated protein degradation (ERAD) pathway, directly targeting HA biosynthesis as a potential antiviral mechanism (Frabutt et al., 2018). Thus, evolution of glycosites with reduced accessibility of nascent glycans to mannosidases and mannosidase-like proteins could inhibit this pathway, leading to enhanced replication. Presence of oligomannose glycans on human IAV HAs may also be relevant to localization of infection within respiratory tissues. IAV infection in humans is typically initiated through exposure to airborne respiratory droplets, resulting in virus binding to  $\alpha$ 2-6-linked receptors on the surface of epithelial cells in the upper airway (Connor et al., 1994; Peng et al., 2017; Rogers and Paulson, 1983; Shinya et al., 2006). It is now well established that primary innate immune defenses against influenza in the respiratory tract consist of secreted host factors, including calcium-dependent (C-type) surfactant proteins SP-A and SP-D (Hartshorn et al., 1994; Nayak et al., 2012; Ng et al., 2012). Notably, SP-D binds specifically to high-mannose type N-glycans (Goh et al., 2013), particularly Man<sub>9</sub>, and confers protection against pathogens containing oligomannose. However, gene expression studies have revealed that SP-D is mainly isolated to the lung and lower respiratory tissues (Su et al., 2004), thus human-adapted IAVs that primarily target the upper respiratory tract are able to increase high-mannose N-glycan expression while still evading host immune defenses.

Further to potential biological rationales for shifts favoring oligomannose glycosylation in human IAV HAs, we were also interested in the structural and molecular basis of how these modifications arise since directly comparable glycosites feature highly diverse occupancies on different HAs. While the presence of under-processed oligomannose rich glycosites on the influenza HA is consistent with mechanisms leading to steric

interference of the biosynthetic processing pathway, our observations were unexpected since HA is substantially less glycosylated than the surface glycoproteins of numerous other viruses. With up to thirty N-linked glycans per monomer, both HIV gp120 and MERS CoV S-2P are well-characterized examples that comprise numerous oligomannose sites arising due to close packing of their many structurally proximal glycosites (Cao et al., 2017, 2018). By contrast, HA glycans are far fewer and appear sparsely arranged (Figure 4), suggesting that in this case, presence of oligomannose glycans is not due to steric restrictions imposed by neighboring glycan chains. We have found that appearance of glycosites with significant high-mannose incorporation in HA is more strongly associated with global placement on the molecule, particularly when located within the head domain, and with local structural and/or sequence adaptations that serve to alter the positioning or conformation of the attached glycan. Observations that some high-mannose glycans span the gap between protomers within the HA trimer, notably N165 in Vic/11 H3 and N169 in Viet/04 H5 (Figure 4), also suggests a potential role in stabilizing subunit interactions and has been posited for influenza NA (Nagae and Yamaguchi, 2012).

Increased oligomannose glycoforms on the head domain of human IAV HAs is particularly relevant to seasonal H3N2 viruses, where vaccine protection has reduced significantly in recent years due to substantial antigenic drift and mismatching between egg-grown vaccines and circulating strains. In this regard, it is of interest that GNL is able to neutralize recent H3 viruses independent of antigenic variances, underscoring HA glycosylation as a potentially important consideration for future human vaccines and therapeutic mAb development (a small number of papers have reported anti-HA antibodies that make direct contact with head-domain glycans [Barbey-Martin et al., 2002; Iba et al., 2014]). Although plant-derived lectins are not typically suitable as therapeutics due to substantial adsorption to host tissue often leading to inflammatory side effects, the notable efficacy of comparable reagents Banlec (Banana lectin) (Swanson et al., 2015, 2010) and Griffithsin (algal lectin from *Griffithsia* sp.) (Lusvarghi and Bewley, 2016) against HIV and influenza infection, the latter of which has recently entered clinical trials (National Institutes of Health, 2019), certainly provides an interesting precedent for adaptation of these lectins for pharmaceutical application. In this regard, a recent report describes an engineered Banlec that exhibits anti-influenza activity in mice and is extremely well tolerated (Covés-Datson et al., 2020).

While our study adds significantly to the number of IAV HAs for which site-specific glycome data are now available, these results still focus on comparatively isolated examples and clearly substantial further investigation will be required to determine links between enhanced high-mannose glycosylation and HAs with apparent adaptation to human hosts. Development of vaccine and analogous strategies that better take into account HA glycosylation status will likely enhance protection, especially within highly glycosylated human seasonal IAV strains and contribute toward the goal of universal influenza vaccines. Furthermore, that GNL is also able to universally label HA and IAV samples on glycan microarrays provides a significant advance in our ability to screen receptor-binding profiles in new and emerging virus strains and may well contribute to ongoing surveillance efforts.

## STAR★METHODS

Detailed methods are provided in the online version of this paper and include the following:

- [KEY RESOURCES TABLE](#)
- [LEAD CONTACT AND MATERIALS AVAILABILITY](#)
- [EXPERIMENTAL MODEL AND SUBJECT DETAILS](#)
  - Cell Cultures
  - Influenza Virus
- [METHOD DETAILS](#)
  - HA Expression and Purification
  - Glycoproteomics
  - Glycan Arrays
  - HAI and Virus Neutralization Assays
  - MD and Glycan Modelling
- [QUANTIFICATION AND STATISTICAL ANALYSIS](#)
- [DATA AND CODE AVAILABILITY](#)

## SUPPLEMENTAL INFORMATION

Supplemental Information can be found online at <https://doi.org/10.1016/j.chom.2020.03.009>.

## ACKNOWLEDGMENTS

A.J.T. is an EMBO long-term postdoctoral fellowship recipient (ALTF 963-2014). This work was supported by NIH grants (R01 AI114730 & R01 AI113867 [J.C.P.], and P41 GM103533 [J.R.Y.]) and the Kwang Hua Educational Foundation (J.C.P.). We thank Dr. Robb de Vries, Dr. Netanel Tzurum, and Prof. Ian Wilson for various HA genes; Dr. Wenjie Peng and Dr. Corwin Nycholat for contributions to the Paulson lab sialoside array; and Prof. Yoshihiro Kawaoka and the Centers for Disease Control and Prevention for Anhui/13 and NC/99 virus samples, respectively. We gratefully acknowledge services provided by the International Reagent Resource (IRR) for all other virus and antibody samples utilized in this study.

## AUTHOR CONTRIBUTIONS

A.J.T. and J.C.P. conceived and designed the project. A.J.T. designed and conducted experiments, purified HA proteins, and grew and characterized all virus stocks. L.C., Y.M., X.W., J.K.D., and J.R.Y. performed and analyzed glycoproteomic MS analysis. C.K., S.W., C.W., and R.M. manufactured glycan arrays and assisted with data collection, analysis, and validation. A.J.T. and J.C.P. wrote the manuscript, and all authors assisted with editing.

## DECLARATION OF INTERESTS

The authors declare no competing interests.

Received: December 2, 2019

Revised: February 13, 2020

Accepted: March 17, 2020

Published: April 15, 2020

## REFERENCES

- Air, G.M. (1981). Sequence relationships among the hemagglutinin genes of 12 subtypes of influenza A virus. *Proc. Natl. Acad. Sci. USA* 78, 7639–7643.
- Altman, M.O., Angel, M., Košík, I., Trovão, N.S., Zost, S.J., Gibbs, J.S., Casalino, L., Amaro, R.E., Hensley, S.E., Nelson, M.I., and Yewdell, J.W. (2019). Human influenza A virus hemagglutinin glycan evolution follows a temporal pattern to a glycan limit. *mBio* 10, e00204–19.
- Andrabi, R., Bhiman, J.N., and Burton, D.R. (2018). Strategies for a multi-stage neutralizing antibody-based HIV vaccine. *Curr. Opin. Immunol.* 53, 143–151.

- Barbey-Martin, C., Gigant, B., Bizebard, T., Calder, L.J., Wharton, S.A., Skehel, J.J., and Knossow, M. (2002). An antibody that prevents the hemagglutinin low pH fusogenic transition. *Virology* 294, 70–74.
- Blijlevens, J.S., Boonstra, S., Onck, P.R., van der Giessen, E., and van Oijen, A.M. (2016). Mechanisms of influenza viral membrane fusion. *Semin. Cell Dev. Biol.* 60, 78–88.
- Cao, L., Diedrich, J.K., Kulp, D.W., Pauthner, M., He, L., Park, S.R., Sok, D., Su, C.Y., Delahunty, C.M., Menis, S., et al. (2017). Global site-specific N-glycosylation analysis of HIV envelope glycoprotein. *Nat. Commun.* 8, 14954.
- Cao, L., Diedrich, J.K., Ma, Y., Wang, N., Pauthner, M., Park, S.R., Delahunty, C.M., McLellan, J.S., Burton, D.R., Yates, J.R., and Paulson, J.C. (2018). Global site-specific analysis of glycoprotein N-glycan processing. *Nat. Protoc.* 13, 1196–1212.
- Chambers, B.S., Parkhouse, K., Ross, T.M., Alby, K., and Hensley, S.E. (2015). Identification of hemagglutinin residues responsible for H3N2 antigenic drift during the 2014–2015 influenza season. *Cell Rep* 12, 1–6.
- Chen, L.M., Blixt, O., Stevens, J., Lipatov, A.S., Davis, C.T., Collins, B.E., Cox, N.J., Paulson, J.C., and Donis, R.O. (2012). In vitro evolution of H5N1 avian influenza virus toward human-type receptor specificity. *Virology* 422, 105–113.
- Chen, L.M., Rivailleur, P., Hossain, J., Carney, P., Balish, A., Perry, I., Davis, C.T., Garten, R., Shu, B., Xu, X., et al. (2011). Receptor specificity of subtype H1 influenza A viruses isolated from swine and humans in the United States. *Virology* 412, 401–410.
- Connor, R.J., Kawaoka, Y., Webster, R.G., and Paulson, J.C. (1994). Receptor specificity in human, avian, and equine H2 and H3 influenza virus isolates. *Virology* 205, 17–23.
- Covés-Datson, E.M., King, S.R., Legendre, M., Gupta, A., Chan, S.M., Gitlin, E., Kulkarni, V.V., Pantaleón García, J., Smee, D.F., Lipka, E., et al. (2020). A molecularly engineered antiviral banana lectin inhibits fusion and is efficacious against influenza virus infection in vivo. *Proc. Natl. Acad. Sci. USA* 117, 2122–2132.
- de Graaf, M., and Fouchier, R.A. (2014). Role of receptor binding specificity in influenza A virus transmission and pathogenesis. *EMBO J* 33, 823–841.
- de Vries, R.P., Peng, W., Grant, O.C., Thompson, A.J., Zhu, X., Bouwman, K.M., de la Pena, A.T.T., van Breemen, M.J., Ambeepitiya Wickramasinghe, I.N., de Haan, C.A.M., et al. (2017a). Three mutations switch H7N9 influenza to human-type receptor specificity. *PLoS Pathog* 13, e1006390.
- de Vries, R.P., Tzurum, N., Peng, W., Thompson, A.J., Ambeepitiya Wickramasinghe, I.N., de la Pena, A.T.T., van Breemen, M.J., Bouwman, K.M., Zhu, X., McBride, R., et al. (2017b). A single mutation in Taiwanese H6N1 influenza hemagglutinin switches binding to human-type receptors. *EMBO Mol. Med.* 9, 1314–1325.
- de Vries, R.P., Zhu, X., McBride, R., Rigter, A., Hanson, A., Zhong, G., Hatta, M., Xu, R., Yu, W., Kawaoka, Y., et al. (2014). Hemagglutinin receptor specificity and structural analyses of respiratory droplet-transmissible H5N1 viruses. *J. Virol.* 88, 768–773.
- Elbein, A.D., Dorling, P.R., Vosbeck, K., and Horisberger, M. (1982). Swainsonine prevents the processing of the oligosaccharide chains of influenza virus hemagglutinin. *J. Biol. Chem.* 257, 1573–1576.
- Eng, J.K., McCormack, A.L., and Yates, J.R. (1994). An approach to correlate tandem mass spectral data of peptides with amino acid sequences in a protein database. *J. Am. Soc. Mass Spectrom.* 5, 976–989.
- Erbelding, E.J., Post, D.J., Stemny, E.J., Roberts, P.C., Augustine, A.D., Ferguson, S., Paules, C.I., Graham, B.S., and Fauci, A.S. (2018). A universal influenza vaccine: the strategic plan for the national institute of allergy and infectious diseases. *J. Infect. Dis.* 218, 347–354.
- Fernández de Toro, B., Peng, W., Thompson, A.J., Domínguez, G., Cañada, F.J., Pérez-Castells, J., Paulson, J.C., Jiménez-Barbero, J., and Canales, Á. (2018). Avenues to characterize the interactions of extended N-glycans with proteins by NMR spectroscopy: the influenza hemagglutinin case. *Angew. Chem. Int. Ed. Engl.* 57, 15051–15055.
- Frabutt, D.A., Wang, B., Riaz, S., Schwartz, R.C., and Zheng, Y.H. (2018). Innate sensing of influenza A virus hemagglutinin glycoproteins by the host endoplasmic reticulum (ER) stress pathway triggers a potent antiviral response via ER-associated protein degradation. *J. Virol.* 92, e01690–17.
- Garten, R.J., Davis, C.T., Russell, C.A., Shu, B., Lindstrom, S., Balish, A., Sessions, W.M., Xu, X., Skepner, E., Deyde, V., et al. (2009). Antigenic and genetic characteristics of swine-origin 2009 A(H1N1) influenza viruses circulating in humans. *Science* 325, 197–201.
- Gatlin, C.L., Eng, J.K., Cross, S.T., Detter, J.C., and Yates, J.R., 3rd. (2000). Automated identification of amino acid sequence variations in proteins by HPLC/microspray tandem mass spectrometry. *Anal. Chem.* 72, 757–763.
- Goh, B.C., Rynkiewicz, M.J., Cafarella, T.R., White, M.R., Hartshorn, K.L., Allen, K., Crouch, E.C., Calin, O., Seeger, P.H., Schultheis, K., and Seaton, B.A. (2013). Molecular mechanisms of inhibition of influenza by surfactant protein D revealed by large-scale molecular dynamics simulation. *Biochemistry* 52, 8527–8538.
- Hartshorn, K.L., Crouch, E.C., White, M.R., Eggleton, P., Tauber, A.I., Chang, D., and Sastry, K. (1994). Evidence for a protective role of pulmonary surfactant protein D (SP-D) against influenza A viruses. *J. Clin. Invest.* 94, 311–319.
- Herfst, S., Schrauwen, E.J., Linster, M., Chutinimitkul, S., de Wit, E., Munster, V.J., Sorrell, E.M., Bestebroer, T.M., Burke, D.F., Smith, D.J., et al. (2012). Airborne transmission of influenza A/H5N1 virus between ferrets. *Science* 336, 1534–1541.
- Iba, Y., Fujii, Y., Ohshima, N., Sumida, T., Kubota-Koketsu, R., Ikeda, M., Wakiyama, M., Shirouzu, M., Okada, J., Okuno, Y., et al. (2014). Conserved neutralizing epitope at globular head of hemagglutinin in H3N2 influenza viruses. *J. Virol.* 88, 7130–7144.
- Imai, M., and Kawaoka, Y. (2012). The role of receptor binding specificity in interspecies transmission of influenza viruses. *Curr. Opin. Virol.* 2, 160–167.
- Imai, M., Watanabe, T., Hatta, M., Das, S.C., Ozawa, M., Shinya, K., Zhong, G., Hanson, A., Katsura, H., Watanabe, S., et al. (2012). Experimental adaptation of an influenza H5 HA confers respiratory droplet transmission to a reassortant H5 HA/H1N1 virus in ferrets. *Nature* 486, 420–428.
- Imai, M., Watanabe, T., Kiso, M., Nakajima, N., Yamayoshi, S., Iwatsuki-Horimoto, K., Hatta, M., Yamada, S., Ito, M., Sakai-Tagawa, Y., et al. (2017). A highly pathogenic avian H7N9 influenza virus isolated from a human is lethal in some ferrets infected via respiratory droplets. *Cell Host Microbe* 22, 615–626.e8.
- Kaku, H., and Goldstein, I.J. (1989). [27] Snowdrop lectin. In *Methods in Enzymology*, 179 (Academic Press), pp. 327–331.
- Khatri, K., Klein, J.A., White, M.R., Grant, O.C., Leymarie, N., Woods, R.J., Hartshorn, K.L., and Zaia, J. (2016). Integrated omics and computational glycobiology reveal structural basis for influenza A virus glycan microheterogeneity and host interactions. *Mol. Cell. Proteomics* 15, 1895–1912.
- Killingley, B., and Nguyen-Van-Tam, J. (2013). Routes of influenza transmission. *Infl. Other Respir. Viruses* 7, 42–51.
- Kirschner, K.N., Yonge, A.B., Tschampel, S.M., González-Outeiriño, J., Daniels, C.R., Foley, B.L., and Woods, R.J. (2008). GLYCAMS: a generalizable biomolecular force field. *Carbohydrates. J. Comp. Chem.* 29, 622–655.
- Kolarich, D., Rapp, E., Struwe, W.B., Haslam, S.M., Zaia, J., McBride, R., Agravat, S., Campbell, M.P., Kato, M., Ranzinger, R., et al. (2013). The minimum information required for a glycomics experiment (MIRAGE) project: improving the standards for reporting mass-spectrometry-based glycoanalytic data. *Mol. Cell. Proteomics* 12, 991–995.
- Krammer, F., Smith, G.J.D., Fouchier, R.A.M., Peiris, M., Kedzierska, K., Doherty, P.C., Palese, P., Shaw, M.L., Treanor, J., Webster, R.G., and García-Sastre, A. (2018). Influenza. *Nat. Rev. Dis. Prim.* 4, 3.
- Linster, M., van Boheemen, S., de Graaf, M., Schrauwen, E.J.A., Lexmond, P., Mänz, B., Bestebroer, T.M., Baumann, J., van Riel, D., Rimmelzaan, G.F., et al. (2014). Identification, characterization, and natural selection of mutations driving airborne transmission of A/H5N1 virus. *Cell* 157, 329–339.
- Liu, Y., McBride, R., Stoll, M., Palma, A.S., Silva, L., Agravat, S., Aoki-Kinoshita, K.F., Campbell, M.P., Costello, C.E., Dell, A., et al. (2017). The minimum information required for a glycomics experiment (MIRAGE) project: improving the standards for reporting glycan microarray-based data. *Glycobiology* 27, 280–284.

- Lusvarghi, S., and Bewley, C.A. (2016). Griffithsin: an antiviral lectin with outstanding therapeutic potential. *Viruses* 8, E296.
- Mir-Shekari, S.Y., Ashford, D.A., Harvey, D.J., Dwek, R.A., and Schulze, I.T. (1997). The glycosylation of the influenza A virus hemagglutinin by mammalian cells. A site-specific study. *J. Biol. Chem.* 272, 4027–4036.
- Nagae, M., and Yamaguchi, Y. (2012). Function and 3D structure of the N-glycans on glycoproteins. *Int. J. Mol. Sci.* 13, 8398–8429.
- Nakamura, K., Bhowm, A.S., and Compans, R.W. (1980). Glycosylation sites of influenza viral glycoproteins. Tryptic glycopeptides from the A/WSN (H0N1) hemagglutinin glycoprotein. *Virology* 107, 208–221.
- National Institutes of Health. (2019). Griffithsin-based rectal microbicide for PREvention of viral ENTry (PREVENT). <https://clinicaltrials.gov/ct2/show/NCT04032717>.
- Nayak, A., Dodagatta-Marri, E., Tsolaki, A.G., and Kishore, U. (2012). An insight into the diverse roles of surfactant proteins, SP-A and SP-D in innate and adaptive immunity. *Front. Immunol.* 3, 131.
- Neumann, G., and Kawaoka, Y. (2015). Transmission of influenza A viruses. *Virology* 479–480, 234–246.
- Ng, W.C., Tate, M.D., Brooks, A.G., and Reading, P.C. (2012). Soluble host defense lectins in innate immunity to influenza virus. *J. Biomed. Biotechnol.* 2012, 732191.
- Nobusawa, E., Aoyama, T., Kato, H., Suzuki, Y., Tateno, Y., and Nakajima, K. (1991). Comparison of complete amino acid sequences and receptor-binding properties among 13 serotypes of hemagglutinins of influenza A viruses. *Virology* 182, 475–485.
- Pan, Y.T., Hori, H., Saul, R., Sanford, B.A., Molyneux, R.J., and Elbein, A.D. (1983). Castanospermine inhibits the processing of the oligosaccharide portion of the influenza viral hemagglutinin. *Biochemistry* 22, 3975–3984.
- Parsons, L.M., An, Y., de Vries, R.P., de Haan, C.A.M., and Cipollo, J.F. (2017). Glycosylation characterization of an influenza H5N7 hemagglutinin series with engineered glycosylation patterns: implications for structure–function relationships. *J. Proteome Res.* 16, 398–412.
- Paules, C., and Subbarao, K. (2017). Influenza. *Lancet* 390, 697–708.
- Peng, W., de Vries, R.P., Grant, O.C., Thompson, A.J., McBride, R., Tsogtbaatar, B., Lee, P.S., Razi, N., Wilson, I.A., Woods, R.J., and Paulson, J.C. (2017). Recent H3N2 viruses have evolved specificity for extended, branched human-type receptors, conferring potential for increased avidity. *Cell Host Microbe* 21, 23–34.
- Rogers, G.N., and Paulson, J.C. (1983). Receptor determinants of human and animal influenza virus isolates: differences in receptor specificity of the H3 hemagglutinin based on species of origin. *Virology* 127, 361–373.
- Rogers, G.N., Paulson, J.C., Daniels, R.S., Skehel, J.J., Wilson, I.A., and Wiley, D.C. (1983). Single amino acid substitutions in influenza haemagglutinin change receptor binding specificity. *Nature* 304, 76–78.
- Shinya, K., Ebina, M., Yamada, S., Ono, M., Kasai, N., and Kawaoka, Y. (2006). Avian flu: influenza virus receptors in the human airway. *Nature* 440, 435–436.
- Smith, G.J.D., Vijaykrishna, D., Bahl, J., Lycett, S.J., Worobey, M., Pybus, O.G., Ma, S.K., Cheung, C.L., Raghwan, J., Bhatt, S., et al. (2009). Origins and evolutionary genomics of the 2009 swine-origin H1N1 influenza A epidemic. *Nature* 459, 1122–1125.
- Srinivasan, K., Raman, R., Jayaraman, A., Viswanathan, K., and Sasisekharan, R. (2013). Quantitative characterization of glycan-receptor binding of H9N2 influenza A virus hemagglutinin. *PLoS One* 8, e59550.
- Struwe, W.B., Agravat, S., Aoki-Kinoshita, K.F., Campbell, M.P., Costello, C.E., Dell, A., Ten Feizi, F., Haslam, S.M., Karlsson, N.G., Khoo, K.H., et al. (2016). The minimum information required for a glycomics experiment (MIRAGE) project: sample preparation guidelines for reliable reporting of glycomics datasets. *Glycobiology* 26, 907–910.
- Su, A.I., Wilshire, T., Batalov, S., Lapp, H., Ching, K.A., Block, D., Zhang, J., Soden, R., Hayakawa, M., Kreiman, G., et al. (2004). A gene atlas of the mouse and human protein-encoding transcriptomes. *Proc. Natl. Acad. Sci. USA* 101, 6062–6067.
- Swanson, M.D., Boudreaux, D.M., Salmon, L., Chugh, J., Winter, H.C., Meagher, J.L., André, S., Murphy, P.V., Oscarson, S., Roy, R., et al. (2015). Engineering a therapeutic lectin by uncoupling mitogenicity from antiviral activity. *Cell* 163, 746–758.
- Swanson, M.D., Winter, H.C., Goldstein, I.J., and Markovitz, D.M. (2010). A lectin isolated from bananas is a potent inhibitor of HIV replication. *J. Biol. Chem.* 285, 8646–8655.
- Tabb, D.L., McDonald, W.H., and Yates, J.R., 3rd. (2002). DTASelect and contrast: tools for assembling and comparing protein identifications from shotgun proteomics. *J. Proteome Res.* 1, 21–26.
- Tumpey, T.M., Maines, T.R., Van Hoeven, N., Glaser, L., Solórzano, A., Pappas, C., Cox, N.J., Swaine, D.E., Palese, P., Katz, J.M., and García-Sastre, A. (2007). A two-amino acid change in the hemagglutinin of the 1918 influenza virus abolishes transmission. *Science* 315, 655–659.
- Tzurum, N., de Vries, R.P., Peng, W., Thompson, A.J., Bouwman, K.M., McBride, R., Yu, W., Zhu, X., Verheijen, M.H., Paulson, J.C., and Wilson, I.A. (2017). The 150-loop restricts the host specificity of human H1N8 influenza virus. *Cell Rep* 19, 235–245.
- Ward, C.W., and Dopheide, T.A. (1981a). Amino acid sequence and oligosaccharide distribution of the haemagglutinin from an early Hong Kong influenza virus variant A/Aichi/2/68 (X-31). *Biochem. J.* 193, 953–962.
- Ward, C.W., and Dopheide, T.A. (1981b). Evolution of the Hong Kong influenza A sub-type. Structural relationships between the haemagglutinin from A/duck/Ukraine/1/63 (Hav 7) and the Hong Kong (H3) haemagglutinins. *Biochem. J.* 195, 337–340.
- Ward, C.W., Gleeson, P.A., and Dopheide, T.A. (1980). Carbohydrate composition of the oligosaccharide units of the haemagglutinin from the Hong Kong influenza virus A/Memphis/102/72. *Biochem. J.* 189, 649–652.
- Webster, R.G., Bean, W.J., Gorman, O.T., Chambers, T.M., and Kawaoka, Y. (1992). Evolution and ecology of influenza A viruses. *Microbiol. Rev.* 56, 152–179.
- Woods Group (2005–2019). GLYCAM web (Complex Carbohydrate Research Center (University of Georgia).
- Wormald, M.R., Petrescu, A.J., Pao, Y.L., Glithero, A., Elliott, T., and Dwek, R.A. (2002). Conformational studies of oligosaccharides and glycopeptides: complementarity of NMR, X-ray crystallography, and molecular modelling. *Chem. Rev.* 102, 371–386.
- Xu, T., Park, S.K., Venable, J.D., Wohlschlegel, J.A., Diedrich, J.K., Cociorva, D., Lu, B., Liao, L., Hewel, J., Han, X., et al. (2015). ProLuCID: an improved SEQUEST-like algorithm with enhanced sensitivity and specificity. *J. Proteomics* 129, 16–24.
- Yamada, S., Suzuki, Y., Suzuki, T., Le, M.Q., Nidom, C.A., Sakai-Tagawa, Y., Muramoto, Y., Ito, M., Kiso, M., Horimoto, T., et al. (2006). Haemagglutinin mutations responsible for the binding of H5N1 influenza A viruses to human-type receptors. *Nature* 444, 378–382.
- York, W.S., Agravat, S., Aoki-Kinoshita, K.F., McBride, R., Campbell, M.P., Costello, C.E., Dell, A., Feizi, T., Haslam, S.M., Karlsson, N., et al. (2014). Mirage: the minimum information required for a glycomics experiment. *Glycobiology* 24, 402–406.
- Zhang, M., Gaschen, B., Blay, W., Foley, B., Haigwood, N., Kuiken, C., and Korber, B. (2004). Tracking global patterns of N-linked glycosylation site variation in highly variable viral glycoproteins: HIV, SIV, and HCV envelopes and influenza hemagglutinin. *Glycobiology* 14, 1229–1246.
- Ziegler, T., Mamahit, A., and Cox, N.J. (2018). 65 years of influenza surveillance by a World Health Organization-coordinated global network. *Influ. Other Respir. Viruses* 12, 558–565.
- Zost, S.J., Parkhouse, K., Gumina, M.E., Kim, K., Diaz Perez, S., Wilson, P.C., Treanor, J.J., Sant, A.J., Cobey, S., and Hensley, S.E. (2017). Contemporary H3N2 influenza viruses have a glycosylation site that alters binding of antibodies elicited by egg-adapted vaccine strains. *Proc. Natl. Acad. Sci. USA* 114, 12578–12583.

## STAR★METHODS

## KEY RESOURCES TABLE

REAGENT or RESOURCE	SOURCE	IDENTIFIER
<b>Antibodies</b>		
Anti-HIS mouse antibody	Thermo Fisher Scientific	Cat# MA1-21315; RRID:AB_557403
Alexa488-linked anti-mouse IgG	Thermo Fisher Scientific	Cat# A-11029; RRID:AB_138404
Alexa488-linked anti-sheep IgG	Thermo Fisher Scientific	Cat# A-11015; RRID:AB_141362
anti-Cal/04 clone AT171.718.57	International Reagent Resource	Cat# FR507
anti-Per/09 clone AT250.12.57	International Reagent Resource	Cat# FR553
anti-Per/09 clone AT250.656.170	International Reagent Resource	Cat# FR557
anti-Bris/07 clone AT179.145.161	International Reagent Resource	Cat# FR509
anti-Bris/07 clone AT179.705.161	International Reagent Resource	Cat# FR510
anti-Bris/07 clone AT179.632.135	International Reagent Resource	Cat# FR511
anti-Bris/07 clone AT179.428.45	International Reagent Resource	Cat# FR512
Anti-Vic/11 clone ATCC004 1E12	International Reagent Resource	Cat# FR1122
Anti-Vic/11 clone ATCC004 6F6	International Reagent Resource	Cat# FR1123
Anti-Vic/11 clone ATCC004 4D7	International Reagent Resource	Cat# FR1124
Anti-Vic/11 clone ATCC004 3D7	International Reagent Resource	Cat# FR1125
Anti-Vic/11 clone ATCC004 1B2	International Reagent Resource	Cat# FR1126
Anti-Anhui/13	(Imai et al., 2017)	N/A
<b>Bacterial and Virus Strains</b>		
A/California/04/2009	International Reagent Resource	Cat# FR371
A/Victoria/361/2011	International Reagent Resource	Cat# FR1061
A/Anhui/1/2013	(Imai et al., 2017)	N/A
A/New Caledonia/20/1999	(Chen et al., 2011)	N/A
A/Brisbane/10/2007	International Reagent Resource	Cat# FR8
A/Perth/16/2009	International Reagent Resource	Cat# FR370
A/Switzerland/9715293/2013	International Reagent Resource	Cat# FR1368
A/Hong Kong/4801/2014	International Reagent Resource	Cat# FR1453
<b>Biological Samples</b>		
Anti-NC/99 sheep antisera	(Chen et al., 2011)	N/A
Turkey red blood cells (5%)	Lampire Biological	Cat# 50-415-691
<b>Chemicals, Peptides, and Recombinant Proteins</b>		
Biotinylated <i>Galanthus nivalis</i> lectin (GNL)	Vector Labs	Cat# B-1245
Alexa488-conjugated streptavidin	Thermo Fisher Scientific	Cat# S11223
<i>Sambucus Nigra</i> Lectin (SNA)	Vector Labs	Cat# L-1300
<i>Erythrina Cristagalli</i> Lectin (ECA)	Vector Labs	Cat# L-1140
Concanavalin A (ConA)	Vector Labs	Cat# L-1000
FITC-conjugated <i>Maackia Amurensis</i> lectin (MAA)	EY Laboratories	Cat# F-7801-2
dNTP mix	Invitrogen	Cat# 18427013
linear PEI (polyethylimine)	Polysciences	Cat# 23966-1
Phosphate-buffered saline (PBS)	Corning	Cat# 21-040-CV
Imidazole	Sigma Aldrich	Cat# I2399-500G
Fetal Bovine Serum (FBS), heat inactivated,	Thermo Fisher Scientific	Cat# 16140071
DMEM, high glucose, pyruvate	Thermo Fisher Scientific	Cat# 11995065
MEM, no glutamine	Thermo Fisher Scientific	Cat# 11090081
Penicillin-Streptomycin	Thermo Fisher Scientific	Cat# 15140122
L-Glutamine (200 mM)	Thermo Fisher Scientific	Cat# 25030081
Geneticin (G418 Sulfate)	Thermo Fisher Scientific	Cat# 10131035

(Continued on next page)

**Continued**

REAGENT or RESOURCE	SOURCE	IDENTIFIER
TPCK-Trypsin	Thermo Fisher Scientific	Cat# 20233
Tween 20	Fisher Scientific	Cat# BP337-50
Urea	MilliporeSigma	Cat# U5128
Ammonium acetate	MilliporeSigma	Cat# A1542
Dithiothreitol (DTT)	Fisher	Cat# BP172-5
Iodoacetamide	MilliporeSigma	Cat# I1149
Arg-C (protease)	Promega	Cat# V1881
Elastase	Promega	Cat# V1891
Subtilisin	MilliporeSigma	Cat# P5380
Trypsin	Promega	Cat# V5111
Chymotrypsin	Promega	Cat# V1061
Endo H	New England Biolabs	Cat# P0702L
PNGase F	New England Biolabs	Cat# P0705S
<sup>18</sup> O-water	MilliporeSigma	Cat# 329878
Critical Commercial Assays		
Q5 High-Fidelity Hot-Start DNA polymerase	New England Biolabs	Cat# M0493S
NEBuilder HiFi DNA Assembly Master Mix	New England Biolabs	Cat# E2621S
NucleoSpin Gel and PCR Clean-Up	Takara	Cat# 740609.240C
QIAprep Spin Miniprep Kit	Qiagen	Cat# 27106
NucleoBond® Xtra Midi Plus EF	Takara	Cat# 740422.50
TMB ELISA Peroxidase Substrate	Rockland	Cat# TMBE-100
Deposited Data		
X-ray coordinates and structure factors	Protein Data Bank	PDB: 3LZG, 4O5N, 2FK0, 4XKD, 4N5J, 4XQO
Gene and amino acid sequences for Cal/07 (H1)	Global Initiative on Sharing All Influenza Data (GISAID)	EPI177294
Gene and amino acid sequences for Vic/11 (H3)	Global Initiative on Sharing All Influenza Data (GISAID)	EPI418017
Gene and amino acid sequences for Viet/04 (H5)	Global Initiative on Sharing All Influenza Data (GISAID)	EPI550316
Gene and amino acid sequences for Tai/13 (H6)	Global Initiative on Sharing All Influenza Data (GISAID)	EPI459855
Gene and amino acid sequences for Shang/13 (H7)	Global Initiative on Sharing All Influenza Data (GISAID)	EPI439502
Gene and amino acid sequences for Jiang/13 (H10)	Global Initiative on Sharing All Influenza Data (GISAID)	EPI497477
Gene and amino acid sequences for Duck/Ukr/63 (H3)	Global Initiative on Sharing All Influenza Data (GISAID)	EPI90390
Gene and amino acid sequences for HK/68 (H3)	Global Initiative on Sharing All Influenza Data (GISAID)	EPI240947
Glycoproteomics MS data (Figures 1 and 6)	MassIVE repository ( <a href="https://massive.ucsd.edu/ProteoSAFe/static/massive.jsp">https://massive.ucsd.edu/ProteoSAFe/static/massive.jsp</a> )	MSV000084953
Experimental Models: Cell Lines		
HEK 293T cells	N/A	N/A
MDCK II cells	ATCC	Cat# CCL-34
MDCK-SIAT1 cells	Sigma-Aldrich	Cat# 05071502-1VL
Experimental Models: Organisms/Strains		
One Shot TOP10 Electrocomp E. Coli	Thermo Fisher Scientific	Cat# C404050
Oligonucleotides		
H5_fwd: 5'-GGC TTC CGT CCT GGC AGG ATC AGA TCA GAT TTG CAT TGG-3'	Invitrogen	N/A

**Continued**

REAGENT or RESOURCE	SOURCE	IDENTIFIER
H5_rev: 5'-TCA TGC GCT TGA TCA GTG ATC CCT CGA GTT TTA CTC CAC-3'	Invitrogen	N/A
H10_fwd: 5'-GGC TTC CGT CCT GGC AGG ATC ACT GGA CAA GAT TTG CCT CG-3'	Invitrogen	N/A
H10_rev: 5'-TCA TGC GCT TGA TCA GTG ATC CCT CGA GGG TCA CTG GAT TG-3'	Invitrogen	N/A
Recombinant DNA		
pCD5-Cal/07 H1	(Peng et al., 2017)	N/A
pCD5-Vic/11 H3	(Peng et al., 2017)	N/A
pFast-Viet/04 H5	(de Vries et al., 2014)	N/A
pCD5-Tai/13 H6	(de Vries et al., 2017b)	N/A
pCD5-Shang/13 H7	(de Vries et al., 2017a)	N/A
pFast-Jiang/13 H10	(Tzurum et al., 2017)	N/A
Software and Algorithms		
GLYCAM: Glycoprotein Builder	<a href="http://glycam.org;">http://glycam.org/</a> ; (Woods Group, 2005–2019)	N/A
Pymol	Schrödinger, LLC	N/A
Other		
1 ml HisTrap FF crude column	GE Healthcare	Cat# 11000458
Sialoside glycan microarray	This paper and (Peng et al., 2017)	N/A

**LEAD CONTACT AND MATERIALS AVAILABILITY**

Further information and requests for resources and reagents should be directed to and will be fulfilled by the Lead Contact, James C. Paulson ([jpaulson@scripps.edu](mailto:jpaulson@scripps.edu)).

Any unique reagents generated in this study are available from the Lead Contact with a completed Materials Transfer Agreement.

**EXPERIMENTAL MODEL AND SUBJECT DETAILS****Cell Cultures**

HEK 293T cells (human embryonic kidney cells, female) were maintained in DMEM medium supplemented with 10% fetal bovine serum (FBS), and 100 U mL<sup>-1</sup> of Penicillin-Streptomycin. MDCK cells (Madin-Darby canine kidney cells, female) were maintained in MEM medium supplemented with 10% FBS, 2 mM L-Glutamine, and 100 U mL<sup>-1</sup> of Penicillin-Streptomycin. MDCK-SIAT1 cells (Madin-Darby canine kidney cells with stable expression of human 2,6-sialyltransferase, female) were maintained in MEM medium supplemented with 10% FBS, 2 mM L-Glutamine, 100 U mL<sup>-1</sup> of Penicillin-Streptomycin, and 1 mg mL<sup>-1</sup> G418 sulfate.

**Influenza Virus**

Live influenza virus seed stocks were obtained from the International Reagent Resource (IRR; [www.internationalreagentresource.org](http://www.internationalreagentresource.org)) and grown in MDCK or MDCK-SIAT1 cultures (approximately 40 million cells per virus) in MEM medium supplemented with, 2 mM L-Glutamine and 100 U mL<sup>-1</sup> of Penicillin-Streptomycin. Cell cultures were washed twice in warm PBS prior to the addition of virus, typically diluted 1:1000 in growth medium. Diluted virus was incubated with cell cultures for 1 hour before being removed and replaced with growth medium supplemented with 2 µg mL<sup>-1</sup> tosyl phenylalanyl chloromethyl ketone (TPCK)-trypsin and further incubated for 72 h. At day 3, culture supernatant was recovered and centrifuged at 1000x g to remove cell debris before final centrifugation at 65,000x g for 2 hours at 4°C to isolate viral pellets. Viral pellets were resuspended in 1 mL PBS supplemented with 5% (w/v) sterile glycerol, aliquoted, and stored at -80°C. For measuring virus titer by the TCID50 (median tissue culture infectious dose) assay, MDCK or MDCK-SIAT1 cells were washed twice with PBS prior to the addition of virus, and viral growth medium supplemented with 2 µg mL<sup>-1</sup> TPCK-trypsin. For measuring viral HA titers (median hemagglutination), virus stocks were diluted in PBS and an equal volume of 0.5% turkey red blood cells added. A/New Caledonia/20/1999 (Chen et al., 2011) and A/Anhui/1/2013 (Imai et al., 2017) aliquots were obtained in BPL-inactivated (beta-propiolactone) form and only characterized by HA titers.

**METHOD DETAILS****HA Expression and Purification**

Genes encoding HA ectodomains (de Vries et al., 2017a, 2017b, 2014; Peng et al., 2017; Tzurum et al., 2017) (residues 11–521; H3 numbering) were cloned into a customized DNA vector for expression in mammalian tissue culture featuring an N-terminal CD5 signal peptide, a C-terminal leucine zipper (GCN4) motif, and His<sub>8</sub>-tag using the NEBuilder HiFi DNA Assembly Master Mix. Final expression constructs were transfected into HEK293T cells using linear PEI (polyethylenimine) at 5:1 w/w. After 12 hours, transfected cells were exchanged into serum-free media and incubated for a further 48 hours at 37°C, 5% CO<sub>2</sub>. Recombinant HA trimers were purified directly from condition media by IMAC using a 1 ml HisTrap FF crude column (GE). HAs were eluted in a gradient of PBS containing 0.5 M (final) imidazole, washed, and concentrated to 0.5–1.0 mg ml<sup>-1</sup> final stock. Amino acid sequences of all HA ectodomains utilized for glycoproteomic analysis are given in [Data S4](#).

**Glycoproteomics**

HAs were digested and deglycosylated as previously described (Cao et al., 2017) (for comprehensive method details see (Cao et al., 2018)). Briefly, approximately 50 µg of each HA was denatured with 8 M urea in 0.1 M ammonium acetate (pH 6), followed by DTT and iodoacetamide treatments to reduce and alkylate the protein. The resulting protein was divided into aliquots for proteolytic digestions, including triple digestion (Gatlin et al., 2000), chymotrypsin, and the combination of trypsin and chymotrypsin. Protease enzymes were then denatured at 100°C for 5 min. Each of the samples generated from different proteolytic digestions was deglycosylated with Endo H, followed by PNGase F treatment. The samples were then analyzed on a Fusion Orbitrap tribrid mass spectrometer (Thermo Fisher Scientific). MS/MS spectra were searched against the European Bioinformatic Institute (IPI) *Bos taurus* protein database, including the sequences of HAs analyzed in this study using the Integrated Proteomics Pipeline Ver. 5.1.2 (Eng et al., 1994; Tabb et al., 2002; Xu et al., 2015). Each peak was smoothed and fitted to Gaussian distribution to calculate the relative abundance of peptide using peak area. Sequence coverage maps and (glyco)peptide assignment data are included in [Data S5](#). Generally, the MIRAGE guidelines were followed throughout all procedures (Kolarich et al., 2013; York et al., 2014).

**Glycan Arrays**

For antibody detection, recombinant HA trimers (50 µg ml<sup>-1</sup> final) were pre-complexed with the anti-His mouse antibody (Thermo Fisher Scientific) and the Alexa488-linked anti-mouse IgG (Thermo Fisher Scientific) at 4:2:1 molar ratio for 15 min on ice in 50 µl PBS-T. This complex was incubated on the array surface in a humidified chamber for 60 min before washing and analysis. For GNL detection, recombinant HA trimers (50 µg ml<sup>-1</sup> final) alone in 50 µl PBS-T were incubated on the array surface in a humidified chamber for 60 min, followed by washing and further incubation with a complex of GNL:Streptavidin-Alexa488 for 60 min. For whole viruses, virus stocks diluted to 256 HAU (final) in PBS, 3% BSA were incubated on the array surface in a humidified chamber for 60 min, followed by washing and incubation with either GNL:Streptavidin-Alexa488 or antiviral monoclonal antibodies or antisera for a final 60 min. Unlabeled antiviral reagents were detected with Alexa488 anti-mouse or anti-sheep secondary antibodies incubating for 60 min. Following final washing, all arrays were scanned using an Innoscan 1100AL microarray scanner (Innopsys). A complete list of the glycans on the array is presented in [Data S1](#). Full descriptions of the microarray experiment and datasets are presented in [Data S2](#) and [S3](#) according to the MIRAGE consortium format (Liu et al., 2017; Struwe et al., 2016).

**HAI and Virus Neutralization Assays**

For HAI, anti-Cal/04 (FR507), anti-Per/09 (FR553), and lectin stocks were diluted to 20 µg ml<sup>-1</sup> before making 2-fold serial dilutions across 96-well U-bottom plates (final concentration range = 10–0.005 µg ml<sup>-1</sup>). Pre-titered Cal/04 (H1N1) and Per/09 (H3N2) viruses were applied to each well at 8 HAU (final) and incubated for 30 min at room temperature. Hemagglutination inhibition was analyzed through addition of 0.5% (final) turkey red blood cells, and titers read after a 30–45-minute incubation at room temperature. All titers were calculated in triplicate and values averaged. For microneutralization, all antibodies and GNL were diluted to 20 µg ml<sup>-1</sup> before making 10-fold serial dilutions (range = 2.0–2.0e<sup>-7</sup> µg ml<sup>-1</sup>) in microtiter plates. Pre-titered Bris/07, Per/09, Vic/11, Switz/13, and HK/14 were applied to each well at 100 TCID<sub>50</sub> ml<sup>-1</sup> (final; in virus media containing TPCK-trypsin) and incubated for 30 min at room temperature. Following incubation, 100 µl of each sample was applied to three wells of a 96-well plate containing MDCK (all viruses except HK/14) or MDCK-SIAT1 (HK/14 only) and incubated for 72 hours. Viral growth/neutralization titers were determined by analyzing CPE and hemagglutination of the final supernatant by mixing 1:1 with 0.5% (final) turkey red blood cells in 96-well U-bottom plates. All microneutralization assays were repeated in biological triplicate and average titers calculated.

**MD and Glycan Modelling**

PDB entries for Cal/04 (3LZG), Vic/11 (4O5N), Viet/04 (2FK0), Tai/13 (4XKD), Shang/13 (4N5J), and Jiang/13 (4XQO) were downloaded and edited manually to remove all non-protein components including ligands, solvent molecules, and a minimal number of paucimannose type glycans from insect cell expression. For glycan modelling, all protein models were edited into two forms, containing either a single HA protomer or one single HA trimer. Protein models were uploaded to the Glycoprotein Builder tool within the web implementation of GLYCAM (Woods Group, 2005–2019) (<http://glycam.org>). Since only one glycoform could be assigned per glycosite, the major (>50% either complex, high-mannose, or no glycan) glycoconjugate as determined in [Figure 1](#) was selected for inclusion to produce a view of a “typical” HA trimer likely present on the surface of each virus. To reduce the complexity of sim-

ulations and minimize over-estimation of the HA glycan footprint, one of three simple, commonly observed glycoforms were selected for oligomannose or complex, and are modeled as either Man<sub>9</sub> (oligomannose >70%), Man<sub>5</sub> (oligomannose >50%), or asialo-LacNAc<sub>1</sub> biantennary glycans (all complex >50%; see [Figure S4](#) for structures). This determination was made since previous studies have shown that glycosites with very high oligomannose occupancy strongly tend towards entirely unprocessed Man<sub>9</sub> glycoforms, whereas lower high-mannose fractions are more commonly observed as Man<sub>5</sub> ([Khatri et al., 2016](#)). Expected rotamer geometries for the Man $\alpha$ 1–6Man $\beta$  bond(s) in both glycans were set as commonly observed forms: gg and gt ( $\omega = 60$  and  $180^\circ$  respectively) ([Fernández de Toro et al., 2018](#); [Wormald et al., 2002](#)). Conformations of all attached glycans were then energy minimized using the GLYCAM06 forcefield ([Kirschner et al., 2008](#)) deployed within Glycoprotein Builder. All final structural and surface figures were assembled in Pymol (Schrödinger, LLC) using fully-glycosylated HA trimers. Majority (>70%) oligomannose and complex glycans were colored green and purple, respectively, while mixed occupancy species are shown in orange.

### QUANTIFICATION AND STATISTICAL ANALYSIS

Fluorescence intensities recorded using Mapix (Innopsys) for glycan microarray experiments in [Figures 2, S1](#), and [S2](#) were quantified via measurement of mean intensity minus mean background of the four median out of six total replicate spots. Data presented is the average of these four replicates with standard error. Statistical analysis is not applied.

### DATA AND CODE AVAILABILITY

All data for glycoproteomics experiments have been uploaded to the MassIVE repository (<https://massive.ucsd.edu/ProteoSAFe/static/massive.jsp>) and are accessible at the following link: <ftp://massive.ucsd.edu/MSV000084953>. All datasets for glycan microarray experiments are attached in Supplementary Tables and [Figures S1–S3](#) according to the MIRAGE consortium format. These datasets have not been uploaded to a public repository since, at present, such a resource does not exist. PDB structure files for glycosylated HA structures generated using GLYCAM and presented in [Figure 4](#) are available from the Lead Contact, James C. Paulson ([jpaulson@scripps.edu](mailto:jpaulson@scripps.edu)), upon request.